Journal of Materials Chemistry A

REVIEW

View Article Online
View Journal | View Issue

Check for updates

Cite this: J. Mater. Chem. A, 2024, 12, 23202

Recent progress on electrocatalysts in ammonia electrooxidation reaction for clean hydrogen production

N. S. Hassan,[ab] A. A. Jalil, *[ab] R. Saravanan, [c] N. M. Izzuddin, [b] M. B. Bahari,[d] D. Prasetyoko [e] and R. E. Nugraha[f]

Hydrogen (H_2) is considered one of the most promising alternative energy resources, serving as a clean energy carrier, replacing fossil fuels. Ammonia (NH_3) is recognized as a high-potential H_2 carrier and is utilized as a primary material for H_2 production. The NH_3 electro-oxidation reaction (AOR) is crucial for both direct NH_3 fuel cells and NH_3 electrolysis. Nevertheless, AOR frequently encounters difficulties including a high overpotential, sluggish reaction rates, and catalyst deactivation as a result of its slow kinetics, even though it is thermodynamically advantageous. In order to overcome these obstacles, numerous approaches have been suggested for the creation of electrocatalysts that can sustain a strong reaction rate even when exposed to low overpotential. The kinetics, mechanisms, and experimental methods of AOR are the primary focus of this overview. It also examines recent advancements in electrocatalyst modifications, with a particular emphasis on single-atom electrocatalysts and transition metal-based catalysts. Additionally, the paper discusses the techno-economic assessment of the AOR reaction for H_2 production. Furthermore, future perspectives and recommendations for electrocatalyst development in AOR are provided. Proposing and designing new, resilient electrocatalysts will be significantly aided by the fundamentals and efforts detailed in this review; this, in turn, will propel advancements in AOR for practical applications.

Received 26th April 2024
Accepted 29th July 2024

DOI: 10.1039/d4ta02897j

rsc.li/materials-a

Published on 07 Mhawuri 2024. Downloaded on 2026-05-14 21:13:42.

Introduction

Fossil fuels, notably coal, oil, and natural gas, have historically served as primary energy sources across various sectors, such as electricity generation, transportation, and industrial processes. However, their finite nature, coupled with significant environmental and social externalities, underscores the imperative for transitioning towards renewable and alternative energy sources. Amidst this transition, hydrogen (H_2) has emerged as a versatile energy carrier with the potential to decarbonize multiple sectors of the economy, including industry, transportation, and power generation.[1,2] While H_2 can be produced through diverse pathways, including electrolysis of water using renewable electricity,[3] biomass gasification,[4] and steam reforming of natural gas coupled with carbon capture and storage,[5] conventional methods often entail carbon-intensive processes or rely on non-renewable resources thus undermining the environmental benefits of H_2 as a clean energy vector.

In this context, the electrooxidation of ammonia (NH_3) presents a promising pathway toward sustainable H_2 production, addressing both environmental and technical challenges associated with conventional methods.[6,7] By harnessing the electrochemical reactivity of NH_3, researchers endeavour to develop efficient and scalable technologies for on-demand H_2 generation, thereby contributing to the transition towards a low-carbon, H_2-based economy. Notably, NH_3 electrooxidation can be conducted under mild conditions, obviating the need for high temperatures and pressures inherent in conventional steam reforming processes.[8] This condition reduces energy consumption and enhances process safety and operational flexibility.

The progression of publications focusing on the electrooxidation of NH_3 from 2008 to 2024, depicted in Fig. 1, underscores the increasing research interest in this area. Notably, 449 documents, including articles, review articles, proceeding papers, and book chapters, have comprehensively explored various aspects of NH_3 electrooxidation over the past 16 years. The surge in publications since 2010 is indicative of significant advancements in research techniques and the perceived

[a]Centre of Hydrogen Energy, Institute of Future Energy, 81310 UTM Johor Bahru, Johor, Malaysia. E-mail: aishahaj@utm.my
[b]Faculty of Chemical and Energy Engineering, Universiti Teknologi Malaysia, 81310 UTM Johor Bahru, Johor, Malaysia
[c]Instituto de Alta Investigación, Universidad de Tarapacá, Arica-1000000, Chile
[d]Faculty of Science, Universiti Teknologi Malaysia, 81310 UTM Johor Bahru, Johor, Malaysia
[e]Department of Chemistry, Faculty of Science and Data Analytics, Institut Teknologi Sepuluh Nopember, Keputih, Sukolilo, Surabaya 60111, Indonesia
[f]Department of Chemical Engineering, Faculty of Engineering, Universitas Pembangunan Nasional "Veteran" Jawa Timur, Surabaya, East Java 60294, Indonesia

This journal is © The Royal Society of Chemistry 2024

Published on 07 Mhawuri 2024. Downloaded on 2026-05-14 21:13:42.

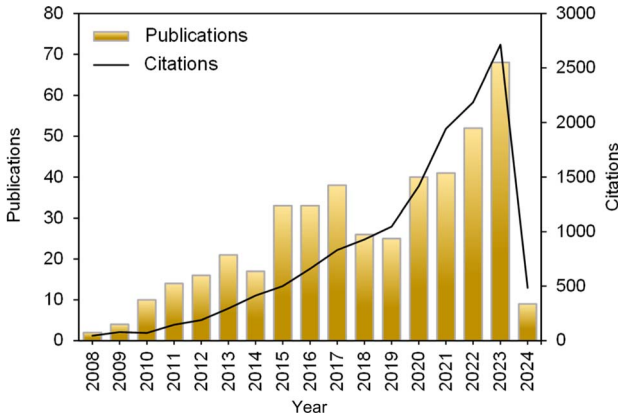

Fig. 1 Publication trends in the area of electrooxidation of NH_3 within 2008–2024.

potential applications of NH_3 electrooxidation in energy conversion, environmental remediation, and chemical synthesis. This surge is also reflected in the increase in citations by 2023. Furthermore, the overlay visualization in Fig. 2 highlights key terms such as "electrooxidation" and "electrochemical oxidation," which stand out with the most significant node sizes, indicating their high frequency of occurrence. Additionally, terms represented by yellow nodes, such as catalysts, electrocatalysts, oxidation, mechanism, and fuel cell, underscore the primary focus of current research.

Indeed, designing electrocatalysts is pivotal in enhancing the efficiency and selectivity of NH_3 electrooxidation. Various materials and strategies have been developed to produce efficient catalysts to replace platinum (Pt),[9] which is costly and scarce. Researchers have explored transition metal-based catalysts, such as nickel (Ni),[10,11] cobalt (Co),[12] and iron (Fe),[13] as promising alternatives due to their abundance and lower cost compared to Pt. Additionally, alloying different metals or incorporating dopants into these materials has been investigated to enhance their catalytic activity and stability. Furthermore, non-metallic materials, such as carbon-based[14] and metal nitrides[15] catalysts have also shown potential for AOR. These

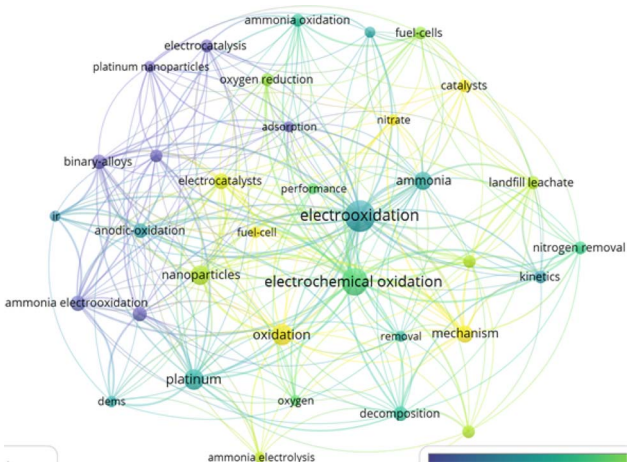

Fig. 2 Overlay visualization of most frequent terms attained *via* VOSViewer v.1.6.19.

materials offer advantages such as high surface area, tunable electronic properties, and chemical stability, making them attractive candidates for electrocatalysis.[16,17] Moreover, nanostructuring and surface engineering techniques have been employed to optimize the morphology and active sites of catalyst materials, further improving their performance in catalysing NH_3 electrooxidation.

Although many reviews cover catalyst development, this review will focus specifically on recent progress in electrocatalyst development to enhance AOR performance. The review will explore the various materials and strategies explored for electrocatalyst design, including single-atom electrocatalysts and transition metal-based catalysts. Additionally, the review will include a techno-economic analysis, assessing the feasibility and cost-effectiveness of different production methods of H_2 for large-scale implementation. Furthermore, the review will discuss the future perspectives and recommendations in electrocatalyst development for AOR. Overall, this review aims to provide insights into the state-of-the-art electrocatalyst design for improving the efficiency and selectivity of NH_3 electrooxidation, contributing to the advancement of sustainable H_2 production technologies.

Ammonia (NH_3) electrolysis for green hydrogen (H_2) production

The utilization of NH_3 as a H_2 carrier undoubtedly is one of the exceptional approaches for the *in situ* production of H_2 fuel. This approach is also noted to exhibit minimal greenhouse gaseous (GHGs) or any hazardous compounds. Besides, NH_3 also displays a promising candidate material for large-scale H_2 production attributed to its high stability and significant capacity for H_2 storage.[18] Concerning these intrinsic features, the production of H_2 from NH_3 has attracted considerable attention and has been deeply studied for its practicability, especially in the industrial process. Interestingly, the transformation of NH_3 to H_2 can be realized using two distinct pathways which are thermal decomposition and electrolysis approaches. Even though the thermal decomposition method is well-known for being more economical compared to electrolysis, the efficiency of this method yet is still inferior to that of the electrolysis method.[19] Moreover, using the high temperature for the decomposition of NH_3 to H_2 and nitrogen constituents will be vulnerable to the formation of GHGs such as nitrous compounds. On the other hand, the electrolysis of NH_3 provides a promising interest in the field of H_2 production. This method utilizes a green technology with no GHGs emissions and it also can achieve high efficiency when powered by renewable energy. The efficiency of this approach also can be further enhanced depending on the advancement of the technology used. Furthermore, thermodynamic calculations demonstrated that the conversion of NH_3 to nitrogen and H_2 requires a negligible quantity of external energy (0.06 V), which is significantly less than the energy demanded by water electrolysis (1.23 V).[20] Theoretically, this indicates that the NH_3 to H_2 conversion is more energy-efficient than water-splitting.[21]

Published on 07 Mhawuri 2024. Downloaded on 2026-05-14 21:13:42.

Generally, the electrolysis of water using renewable electricity and the electrooxidation of ammonia are two distinct processes with different objectives, methodologies, and challenges. The primary purpose of water electrolysis is to produce H_2 and O_2 gases.[22] This process involves splitting water into its constituent elements using an electrical current, with the reaction: $2H_2O \rightarrow 2H_2 + O_2$. The H_2 produced can be used as a clean fuel for various applications, including fuel cells, chemical synthesis, and energy storage. Typically, noble metal catalysts such as platinum (Pt), iridium (Ir), and ruthenium (Ru) are used in this process due to their high activity and stability. The process can utilize either acidic or alkaline electrolytes, and it usually operates at elevated temperatures and pressures to enhance efficiency and gas production rates.[23] The efficiency of water electrolysis systems ranges from 60% to 80%, depending on the specific technology and operating conditions. However, the process requires a high energy input, and challenges include catalyst degradation and overpotential losses. Despite these challenges, water electrolysis is highly suitable for integration with renewable energy sources like solar and wind power, allowing for the storage of intermittent renewable energy in the form of H_2 gas. The environmental impact is minimal, as water is the only by-product, making it a sustainable and environmentally friendly process.

In contrast, the primary purpose of NH_3 electrooxidation is to convert NH_3 to N_2 gas and water helping to treat ammonia-containing waste and reduce environmental pollution. This process typically uses transition metal catalysts such as Pt, Ni, and Cu, which facilitate the oxidation of NH_3. It generally operates at ambient temperature and pressure, making it less energy-intensive than water electrolysis. The efficiency of NH_3 electrooxidation depends on the catalyst used and the reaction conditions. Significant challenges include NH_3 slip (unreacted ammonia), the formation of unwanted by-products, and electrode poisoning. However, this process converts harmful NH_3 into N_2 and water, thereby reducing environmental pollution and preventing ammonia emissions into the atmosphere. NH_3 electrooxidation can also be integrated with renewable energy sources, particularly where NH_3 is produced from renewable H_2, creating a closed-loop sustainable process. Its applications include wastewater treatment and nitrogen removal from industrial effluents, with potential uses in H_2 production.

Briefly, NH_3 electrolysis is a process of dissociating the liquid NH_3 or ammonium in electrochemical cells. Fig. 3 illustrates the basic concept of NH_3 electrolysis. Unlike the photoelectrochemical water-splitting approach, NH_3 electrolysis is a process that is been conducted in the absence of light. This process begins with the direct supply of electricity from the power supply to the system. Typically, in an aqueous NH_3 electrolysis system, as the charges flow through the circuit, the anode electrode undergoes the oxidation of NH_3 to the nitrates compound which then further oxidizes to N_2 molecules. Concurrently, the produced electrons at the anode will be transferred to the cathode electrode for subsequent reduction of water molecules to the H_2 products.[24] On this side, the H_2 evolution reaction (HER) will take place by reducing the water molecules with a consumption of six electron species.

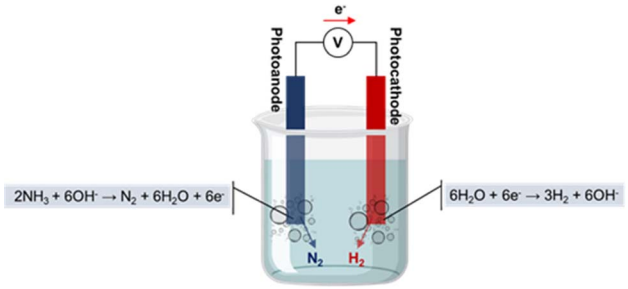

Fig. 3 Principle of electrolysis NH_3 in aqueous solution for H_2 production.

Moreover, the mechanism of NH_3 electrolysis can be described by the equations below:[25]

$$2NH_3 + 6OH^- \rightarrow N_2 + 6H_2O + 6e^- \quad (1)$$

$$6H_2O + 6e^- \rightarrow 3H_2 + 6OH^- \quad (2)$$

Adsorption of NH_3 onto the surface of the catalyst initiates the six-electron in AOR process as well as takes place in an alkaline environment. Significantly, the AOR is traversed *via* two discrete pathways (Fig. 4).[26] Oswin and Salomon introduced the O–S mechanism, a consistent dehydrogenation process, in 1963 as reported by Kim *et al.*[27] In this mechanism, $*NH_3$ on the surface of catalyst undergoes sequential dehydrogenation by OH^- to form *N, which later combines to form N_2. Thus, the O–S mechanism can be described as shown in eqn (3)–(7):

$$NH_{3(aq.)} \rightarrow *NH_3 \quad (3)$$

$$*NH_3 + OH^- \rightarrow *NH_2 + H_2O + e^- \quad (4)$$

$$*NH_2 + OH^- \rightarrow *NH + H_2O + e^- \quad (5)$$

$$*NH + OH^- \rightarrow *N + H_2O + e^- \quad (6)$$

$$*2N \rightarrow N_2 \quad (7)$$

Subsequently to this research, the O–S mechanism was later fine-tuned by Mauerer and Gerischer. Contradict, those

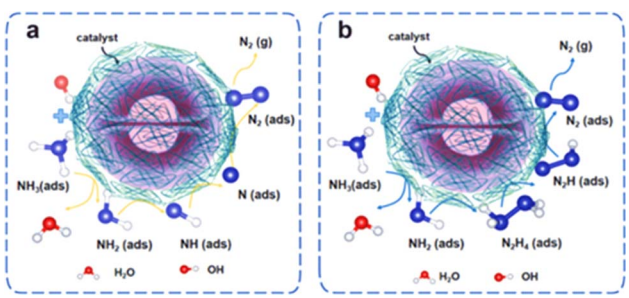

Fig. 4 Oxidation of NH_3 by O–S (a) and G–M (b) mechanism. Reproduced from ref. 26 with permission from Elsevier, copyright 2024.

This journal is © The Royal Society of Chemistry 2024

Published on 07 Mhawuri 2024. Downloaded on 2026-05-14 21:13:42.

researchers proposed that the G–M mechanism in the AOR involves the recombination of $*N_xH_y$ species as well as OH^- dehydrogenation.[28] The G–M mechanism is represented by eqn (8) and (9) below, where $x = 1$ or 2, and $y = 1$ or 2.

$$*NH_x + *NH_y \rightarrow *N_2H_{x+y} \quad (8)$$

$$*N_2H_{x+y} + (x + y)OH^- \rightarrow N_2 + (x + y)H_2O + (x + y)e^- \quad (9)$$

The dehydrogenated *NH and $*NH_2$ were combined to form $*N_2H_{x+y}$. Subsequent dehydrogenation of $*N_2H_{x+y}$ leads to the formation of N_2. In both major mechanisms, the rate-determining step is the dimerization of $*NH_x$ and *N (N_{ads}), which significantly limits the production of N_2 from NH_3 oxidation. However, N_{ads} can be further oxidized by OH^- to generate N–O intermediates, which then form nitrite and nitrate.

$$N_{ads} + OH^- \rightarrow HON_{ads} + e^- \quad (10)$$

$$HON_{ads} + OH^- \rightarrow HONO_{ads} + e^- \quad (11)$$

$$HONO_{ads} + OH^- \rightarrow ONO_{ads} + H_2O + e^- \quad (12)$$

$$ONO_{ads} + OH^- \rightarrow ONO^- (aq.) \quad (13)$$

$$ONO_{ads} + OH^- \rightarrow ONOOH_{ads} + e^- \quad (14)$$

Driven by the catalyst, the OH_{ads} produced in the electrolyte possess high bonding energies, which halts the dimerization process of N_{ads}, leading to their further oxidation to NO_2^- and NO_3^-.[26] During this process, under the influence of OH^- in the electrolyte, the N_{ads} adsorbed on the catalyst surface are gradually hydroxylated to form species such as HON_{ads}, ONO_{ads}, *etc.*, which are then converted to ONOads before being smoothly oxidized to NO_2^- and NO_3^-. For example, the strongly adsorbed N_{ads} hinder the further adsorption of NH_x, resulting in a poor AOR reaction rate. A catalyst, such as CuNi, is expected to exhibit favorable AOR activity for N_2 production only if it possesses appropriate adsorption bonding energy for each intermediate (Fig. 5a and b).[29]

Most research supports the idea that intermediates recombine in the AOR. Additionally, analyses like DEMS and SERS have indicated that N_2 cannot be generated into fully dehydrogenated *N; instead, it acts merely as a poisoning species. Several investigations have linked AOR intermediates to negative health effects, which has sparked discussion over AOR intermediates like $*N_x$, $*N_xH_y$, and $*NO_x$. Accordingly, the key to getting high AOR activity is minimizing poisoning by N_x, NO_x, and N_xH_y and improving the recombination of N_xH_y species.

A straightforward and effective defect-engineering strategy offers a robust approach for AOR mechanistic studies, where oxygen vacancies (Vo) are found to effectively modulate the electronic properties of surface CuO and enhance the binding strength of reaction intermediates.[30] Conventional Pt-based electrocatalysts are generally believed to follow the G–M mechanism because the key intermediate of N_2H_4 was detected. However, the O–S mechanism reaction route *via*

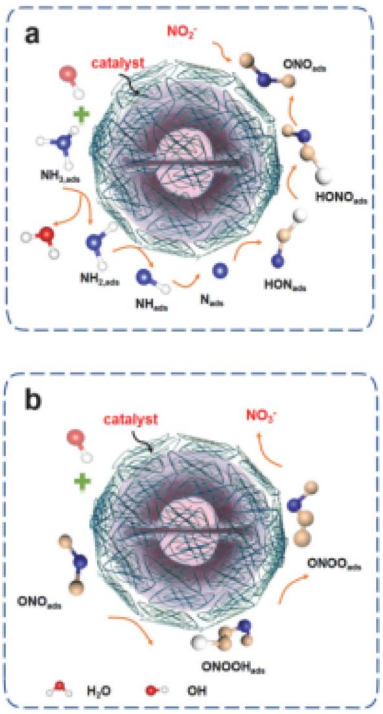

Fig. 5 Ammonia oxidation for the preparation of (a) NO_2^- and (b) NO_3^- mechanism. Reproduced from ref. 26 with permission from Elsevier, copyright 2024.

dehydrogenation of NH_3 to N and N–N coupling is applied to the rich Vo–CuO. Based on the free energy pathway of the AOR process *via* DFT simulations, the NH_3 adsorption process is energetically unfavourable on the Vo-free CuO surface. The free energy changes of the three dehydrogenation steps are all uphill and higher than 1.4 eV due to weak adsorption towards $*NH_x$ species, with the largest free energy change being 1.75 eV, indicating inferior AOR activity (Fig. 6A).[30] However, after introducing the Vo, the free energy of each step decreases by 0.34, 1.84, 2.84, and 2.64 eV, respectively. Additionally, the electronic structures of Cu atoms on the different surface CuO showed that the local density of states of surface Cu atoms move significantly upward towards the Fermi level after introducing Vo, indicating stronger adsorption strength towards the adsorbates. Therefore, the presence of the Vo is beneficial to efficient NH_3 oxidation by stabilizing reaction intermediates. Similarly, Zhang *et al.* claimed that the AOR pathways follow the N + N mechanism containing the N_2H_3 and N_2H_4 intermediate by using TiO–Vo.[32] The introduction of Vo made the N_2 desorption a spontaneous exoergic process, which was a good solution to the most critical catalyst poisoning problem in the AOR process.

Differently, Yang *et al.* reported that CeO_2 with Vo species are the active species in the CeO_x/Y electrode during ammonia electrolysis and follow the G–M mechanism involving the N_2H_4 intermediates (Fig. 6B).[31] Generally, the dehydrogenation of $*NH_3$ to $*NH_2$ is usually the rate-determining step for AOR over metal oxides. In this study, the energy barrier for the conversion of $*NH_3$ to $*NH_2$ on CeO_2 is 2.13 eV, whereas on CeO_2–Vo it is only −0.26 eV, indicating that NH_3 is readily deprotonated. This

Published on 07 Mhawuri 2024. Downloaded on 2026-05-14 21:13:42.

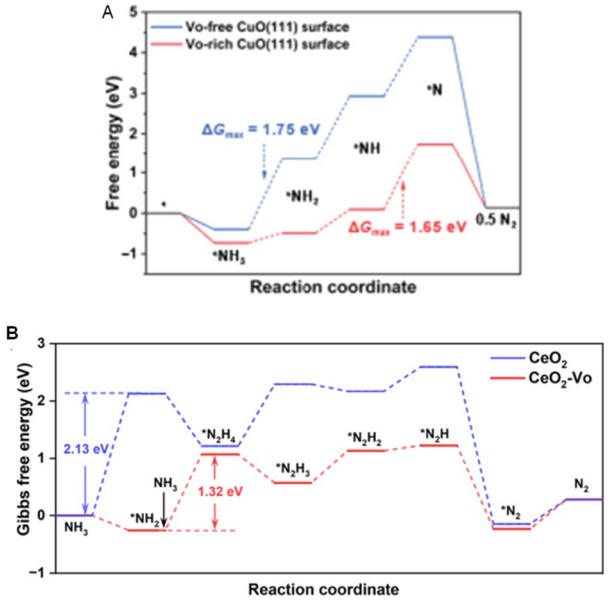

Fig. 6 Free energy diagrams of NH_3 oxidation into N_2 on the (A) Vo-rich and Vo-free CuO *via* O–S mechanism. Reproduced from ref. 30 with permission from Springer, copyright 2022 and (B) CeO_2 and CeO_2–Vo follow the G–M mechanism. Reproduced from ref. 31 with permission from ACS Publications, copyright 2024.

shows that the NH_3 oxidation process is energetically unfavourable on the CeO_2 surface, but the presence of Vo in CeO_2 significantly reduces the energy barrier for $*NH_3$ to $*NH_2$, aligning with the enhanced AOR activity of CeO_2–Vo. When NH_3 adsorbs on Vo sites, one elongated N–H bond points toward a neighboring H atom. The elongation of the N–H bond and the attraction of neighboring O atoms facilitate H transfer. Therefore, it can be concluded that the presence of Vo in CeO_2 not only enhances NH_3 adsorption but also lowers the energy barrier for NH_3 dehydrogenation. This contributes to the increased activity of NH_3 electrolysis following the G–M mechanism.

Achieving high NH_3 electrolysis performance is the main goal for all researchers. Similar to the water-splitting reaction, optimizing the electrochemical cell of NH_3 electrolysis should take into consideration the type, pH and concentration of the electrolyte, and the electrode materials. Frankly speaking, ammonium-based electrolytes such as NH_4Cl, NH_4Br, NH_4I, NH_4NO_3, and NH_4PF_6 are the most suitable electrolytes for NH_3 electrolysis since this process involves the reduction of ammonium species to generate H_2 gas.[33] In addition, the influence of pH on AOR is something that needs to be taken into consideration. Typically, the current density measurement in the AOR rises steadily as the pH goes up, while the starting potential of the anode decreases in line with pH increments. In the study of AOR, alkaline-based electrolytes remain the most commonly used because NH_3 can stay in its molecular form more effectively in these conditions, generally leading to better AOR performance.[26] On the other hand, NH_3 indirect oxidation in acidic media is a very slow process because NH_4^+ is pushed away from the electrodes in acidic ions. Moreover, the oxidation of NH_3 in low pH media often made the anode material susceptible to undesirable corrosion which greatly hampers the AOR process. However, an area of potential interest for AOR is the use of non-aqueous electrolytes, which can eliminate undesirable water oxidation side reactions, narrow AOR potential apertures, and the formation of by-products like nitrates. Therefore, regulating the pH of an AOR system logically is a crucial factor that merits investigation.

Moreover, the concentration of NH_3 in the electrolyte solution also greatly influences the electrolysis performance. Utilising an electrolyte containing a high concentration of NH_3 in this instance can enhance the interaction between NH_3 and the catalyst, resulting in substantial production of H_2. In a recent study, Tran *et al.* observed an enhancement in faradaic efficiency along with an increase in NH_3 concentration.[34] Similarly, Jo *et al.* also found that the AOR performance is directly proportional to the initial concentration of NH_3 which concluded that a high concentration of NH_3 is favorable for high H_2 production.[35] Despite these circumstances, the employment of a high concentration of NH_3 in the electrolysis process might upsurge the overall process cost and unsuitable for large-scale implementation. Therefore, optimization of economic cost and electrolysis performance are substantially important for the systematic design of NH_3 electrolysis systems.

Furthermore, it has been validated that the electrochemical reaction occurring at the anodic electrode constitutes the rate-limiting step in the NH_3-to-H_2 conversion process. Hence, the selection of an appropriate anodic electrode exhibiting outstanding physicochemical and electrical characteristics is imperative. Notably, there exist specific prerequisites to be fulfilled when opting for the anodic material. Primarily, the material must possess elevated physicochemical stability, ensuring minimal or negligible degradation throughout the electrolysis procedure, thereby preserving its original attributes. Additionally, the stability of the anodic material plays a pivotal role in preventing undesired side reactions that could pose environmental hazards and compromise the efficacy of the anodic electrode in the AOR.[36] Moreover, since the anode electrode undergoes an oxidation reaction, the anode must demonstrate exceptional corrosion resistance to ensure an efficient AOR process. Long-term stability of the anodic material during electrolysis is essential for its viability in commercial applications, particularly in industrial processes. Specifically, a high surface area of anode material is desired for the AOR process. The high surface area with exceptional active sites can enhance the surface electrode–electrolyte interface and accelerate the AOR process, ultimately leading to high production of H_2.[26] Electronic properties are of paramount importance, with the anodic material requiring excellent electron and ion transport capabilities to sustain high current densities and minimize energy losses during the process. Lastly, to ensure heightened and efficient AOR activity, the anodic material should exhibit low overpotential values and high selectivity towards N_2 production over NO_x compounds.[34]

Over the years, due to the extraordinary properties of Pt, such as a lower *N affinity than other noble metals and a superior dehydrogenation capacity of NH_x in comparison to non-noble

 This journal is © The Royal Society of Chemistry 2024

Published on 07 Mhawuri 2024. Downloaded on 2026-05-14 21:13:42.

metals, Pt-based materials have garnered considerable interest in the AOR study. This has resulted in superior AOR performance. Nevertheless, the high cost of utilizing Pt has restricted its practical applications. On the other hand, even though non-noble metal demonstrated low AOR efficiency compared to noble metal, its overall efficiency can still be improved by further modification. Therefore, single-atom catalysts and transition-metal-based catalysts have been widely employed for NH_3 electrolysis studies.

Electrocatalysts for AOR in NH_3-to-H_2 conversion

The performance of two classes of AOR catalysts is the primary focus of this section: (1) transition metal-based electrocatalysts and (2) single-atom (SACs) electrocatalysts. Because of their high selectivity, stability, and catalytic activity, SACs electrocatalysts have emerged as promising candidates for NH_3 oxidation. Dispersed on a support material are isolated metal atoms that constitute these catalysts. SACs are distinguished by their electronic and geometric configurations, which enable them to facilitate charge transfer with high efficiency and furnish active sites for the oxidation of NH_3. Recent research has demonstrated the excellent performance of SACs in NH_3 electrooxidation, offering high conversion efficiency and superior selectivity for H_2 production. Additionally, SACs exhibit remarkable stability, making them attractive candidates for practical applications.

Transition metal-based electrocatalysts have also shown promising performance in NH_3 electrooxidation. These electrocatalysts typically consist of transition metal nanoparticles or alloys supported on conductive substrates. Transition metals such as nickel (Ni), cobalt (Co), and copper (Cu) have been extensively studied for NH_3 oxidation due to their high catalytic activity and stability. Transition metal-based electrocatalysts offer several advantages, including tunable electronic properties and high surface area, which enhance catalytic activity and facilitate NH_3 oxidation.[6] Moreover, the abundance and low cost of transition metals make them attractive candidates for large-scale H_2 production *via* AOR. Table 1 shows the summary of single atoms catalysts and transition metal-based electrocatalysts for H_2 production *via* AOR.

Single-atom electrocatalysts

Single-atom catalysts, which comprise an isolated active site composed of a single metal atom, have made significant strides in recent years and have been recognized as the most promising electrocatalysts.[58,59] In contrast to conventional nanoparticle catalysts, the utilization of metal sites in an isolated dispersion maximizes atom utilization. This not only results in a substantial cost reduction but also imparts exceptional catalytic activity and selectivity. The study conducted by Akagi *et al.* examines the potential of anodic catalysts such as Pt, Ru, Ir, Co, Ni, Ta, Fe, and Ti in the electrolysis of liquid NH_3.[33] The current densities were as follows: Ru > Ni > Co > Ir > Pt > Fe at 0.3 V *versus* H_2/NH_3 (Fig. 7A). The AOR reaction on Ti, Ta, Fe, and Co is constrained

Table 1 Single atoms catalyst and transition metal-based electrocatalysts for H_2 production *via* AOR

Catalyst	Current density (mA cm^{-2})	Onset potential (V_{RHE})	Ref.
Ni films	0.45	0.3	33
Pt nanoparticle	1.45	0.9	24
Pt nanosphere	2.6	—	37
Pt/Rh	2.5	0.53	38
Pt/NC	2.4	0.1	39
PtIrCu nanodendrites	122.9 A g^{-1}	0.35	40
PtIrCu nanoframe	—	0.33	41
PtRu/C	0.1	0.2	42
PtIrZn	0.0043	0.3	43
Pt/NiO	0.24	−0.48	44
Pt/TiO_2/S-OLCN	0.28	−0.501	45
Pt/SnO_2/C	—	0.07	14
TM_2@g-CN	—	−0.48	46
RuO_2–ZnO/Al_2O_3	0.74	0.2	47
TiO_2 nanofibers	0.06	0.4	32
NiO–TiO_2	2.93	1.24	10
Co/Ni–C	2.0	0.45	48
$NiCO_2N$ nanoneedle	10	0.71	21
$NiCo_2N$ nanosheets	10	0.55	15
NiCuBO/NF	25	1.301	49
B-NiFe-LDH/NF	100	1.481	50
$Ni(OH)_2$–Cu_2O@CuO	10	0.47	51
$Ni_{1-x}Cu_xOOH$	35	0.28	52
Cu_2O/NF	4.6	0.55	53
Ni_3S_4@$NiCo_2O_4$/NF	50	0.63	54
$LaNi_{0.5}Cu_{0.5}O_{3-\delta}$	10	0.55	55
$La_{1-y}Ni_{0.6}Cu_{0.4-x}Fe_xO_{3-\delta}$	50	0.55	56
$La_{0.5}Sr_{1.5}Ni_{0.9}Cu_{0.1}O_{4-\delta}$	13.4	0.53	57

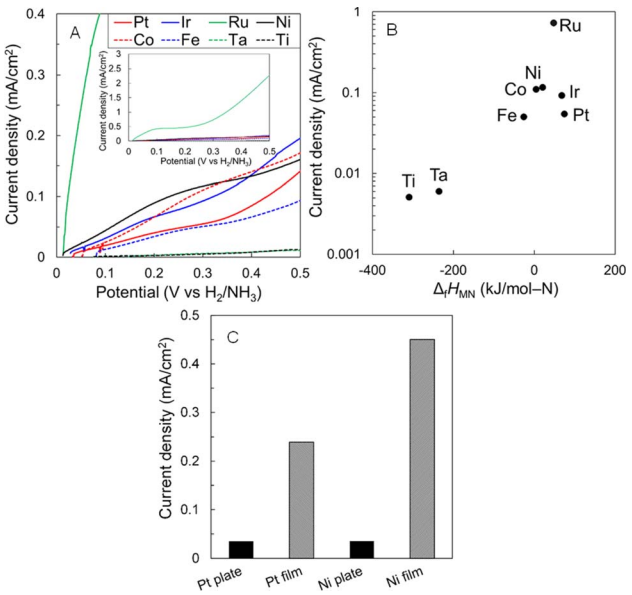

Fig. 7 (A) LSV curves at 10 mV s^{-1}, (B) volcano plot of current density at 0.3 V *vs.* H_2/NH_3 as a function of metal nitride formation enthalpy (Δ_fH_{MN} (kJ mol^{-1} N^{-1})) of various metal plates, and (C) current density for Pt and Ni plates and films for anodic reaction in liquid NH_3 with 0.5 M KNH_2. Reproduced from ref. 33 with permission from Elsevier, copyright 2022.

Published on 07 Mhawuri 2024. Downloaded on 2026-05-14 21:13:42.

by nitrogen desorption, as these elements possess a low metal nitride formation enthalpy (Δ_fH_{MN}) by their high affinity for nitrogen. However, since Ir and Pt have a greater Δ_fH_{MN}, H_2 scission or NH_2-adsorption from NH_x to form N atoms restricts the rate at which they occur. At the apex of the volcano correlation, Ru exhibiting a moderate Δ_fH_{MN} was identified, indicating the greatest catalytic activity[33] (Fig. 7B). Additionally, the authors investigated the impact of Pt and Ni electrode surface configurations, such as plates and films. The current density of the sputtered Pt and Ni films, which possessed a columnar structure and an uneven surface, was observed to be seven and thirteen times greater than that of the Pt and Ni plates, respectively. The sputtered Ni film demonstrated an anodic current density of 0.45 mA cm^{-2} at an anodic potential of 0.3 V *versus* H_2/NH_3 (ref. 33) (Fig. 7C).

The Pt catalyst is the most frequently utilized noble metal catalyst in AOR research.[24] The selection of an ideal electrolyte is critical in optimizing the functionality of electrocatalysts in AOR. In addition to providing the electrolyte with the ions required for the electrochemical reaction, it also affects the stability of the catalyst, the rate of the reaction, and the selectivity of the product. In general, the majority of researchers employed non-aqueous electrolytes; nevertheless, this approach resulted in a rapid decrease in current due to the electrode becoming contaminated with nitride that formed on the anode surface. The incorporation of methanol into the PF_6–DMF (non-aqueous electrolyte), as suggested by Yang *et al.*, significantly improves the electrochemical characteristics of the system, including NH_3 electrolysis stability reduced polarization resistance, and high current density.[41] The NH_3 electrolysis is conducted for 2 hours in the absence of methanol, during which the current density stabilizes at approximately 0.24 mA cm^{-2}. The abrupt increase in current density occurs when 5 wt% methanol is added to the KPF_6–DMF non-aqueous electrolyte. The stabilized current density of 1.45 mA cm^{-2} is exactly six times that of the KPF_6–DMF non-aqueous electrolyte when methanol is not present. Methanol diminishes the intensity of the adsorption of N* species onto the Pt electrode surface, thereby impeding the formation of a nitridation layer.[60]

In recent times, considerable effort has been devoted to modifying the surface orientation and morphologies of Pt particles in an attempt to expose a greater number of active sites. As an illustration, Liu *et al.* investigated different morphologies of Pt architectures including flower, sheet, cauliflower-like shapes, and prickly spheres, to demonstrate that the AOR activity is significantly influenced by the Pt surface morphology. Due to better diffusion control, prickly nanospheres had a current density of 2.6 mA cm^{-2} and better AOR performance than smooth nanoparticles[37] (Fig. 8A). Both the high SSA and the high electrocatalytic activity per unit SSA of smooth, spherical Pt particles explain why they are so much more active as electrocatalysts than hierarchical Pt particles[37] (Fig. 8B). Because of the high electrochemically accessible area of the electrocatalyst and the increase of the interaction with water, nitrogen-doped carbon (2.4 mA cm^{-2}) and Rh surface entities (2.5 mA cm^{-2}) can improve the AOR on Pt nanoparticles.[38,39] An analogous result was observed when PtIrCu

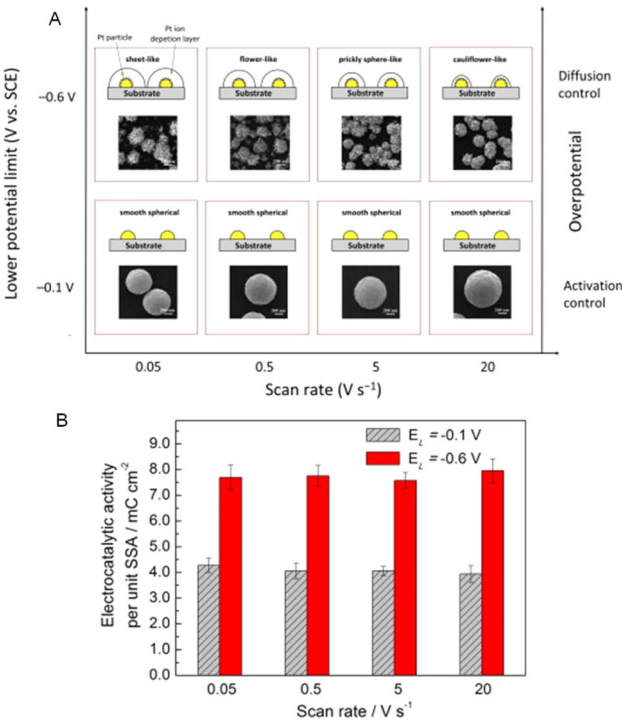

Fig. 8 (A) Schematic representation of a two-dimensional map illustrating how the voltage difference and scan rate affect the particle morphologies; and (B) Pt particles with varied morphologies and EL values of −0.1 V and −0.6 V have varying electrocatalytic activity per unit SSA. Reproduced from ref. 37 with permission from Elsevier, copyright 2013.

hyperbranched concave octahedral nanodendrites improved the electronic effect, exhibiting the highest current density (122.9 A g^{-1}) and the onset potential (0.35 V *vs.* RHE).[40] The exceptional performance of PtIrCu can also be ascribed to the presence of profuse suspended bonds on the high-index facets {553}, {331}, and {221}, which readily interact with NH_3 and promote NH_3 oxidation. In a separate study, Yang *et al.* documented the characteristics of a rhombic dodecahedron nanoframe composed of PtIrCu featuring high-index faceted hyperbranched nanodendrites (RDNF-HNDs). These nanodendrites exhibited a high mass activity of 26.1 A $g_{PtIr}{}^{-1}$ at 0.50 V, which is 7.5 times greater than the mass activity of commercial Pt/C in the AOR 36 and 140 mV lower than RHE.

AOR is influenced by the surface orientation of Pt nanocrystals. AOR occurs mostly on the Pt (100) crystalline plane rather than on the Pt (111) and (110) planes.[14,28,61,62] In contrast to low-index surfaces, high-index crystal surfaces are adorned with an abundance of suspended bonds that facilitate reaction with reactants and thereby augment catalytic activity.[63,64] For AOR, Vidal-Iglesias *et al.* utilized PtMe (Me: Pd, Rh, Ir, Ru) with a particular orientation of Pt (1 0 0) nanoparticles. Out of all the bimetallic samples that were examined, only PtIr and PtRh nanoparticles exhibited an increase in the oxidation density current at low potentials, in contrast to the behavior observed in pure Pt nanoparticles synthesized using the identical technique. PtIr and PtRh nanoparticles, which are preferentially

 This journal is © The Royal Society of Chemistry 2024

Published on 07 Mhawuri 2024. Downloaded on 2026-05-14 21:13:42.

oriented with Pt (100), exhibit greater current densities than polycrystalline Pt nanoparticles. This is because AOR is more sensitive to the presence of square-symmetrical surface sites. On roughened surfaces, however, an increased proportion of exposed Pt(311) planes can substantially increase (by up to 550%) the activity of Pt toward AOR.[65]

Furthermore, one way to manipulate electrical structures is by alloying Pt with other metals.[66] Pt is alloyed with noble metals like PtPd, PtRh, PtRu, and PtIr to increase the AOR's catalytic activity and lower the onset potential by lowering the dehydrogenation reaction's dissociation energy.[42,67–70] The addition of Ir to Pt, for instance, can substantially decrease the activation energy of NH_3 on Pt, thereby decreasing the AOR overpotential.[71] On the other hand, according to the free energy calculations, the onset potential for AOR is lower on Ir compared to Pt. Ir-coated Pt nanocubes, according to Siddharth *et al.*, are the surface-engineered model catalysts for AOR.[9] A comparison of adsorption energies revealed that reaction intermediates, specifically $*NH_3$, bind more strongly to Ir-decorated Pt (100) with a binding energy of −1.68 eV than to Pt (100) with a binding energy of −1.44 eV. This stronger adsorption on Ir-decorated Pt (100) suggests that the catalyst could enhance AOR kinetics. Fig. 9A shows the Gibbs free energy curves for AOR pathways on Pt(100) and Ir-decorated Pt(100). Among the three pathways (N_2H_2, N_2H_3 and N_2H_4), a N_2H_3 pathway is the most favourable one, where the $*NH_2$-to-*NH is the rate-determining step with the energy barrier of 0.96 eV for Pt (100).[9] Interestingly, a reduced energy barrier of 0.74 eV for $*NH_2$-to-*NH step is observed for Ir-decorated Pt(100). They also investigated the optimized structure of AOR intermediates and discovered that there are five optimized structures for favorable N_2H_3 pathways on Ir-decorated Pt(100). Comparing the energy levels in Fig. 9B reveals that a greater binding to the chemical intermediates is facilitated by the surface Ir.[9] Simulation results show that Ir-decorated Pt NCs/C promote reaction intermediate adsorption and lower the energy barrier during the potential determining phase, increasing their activity.

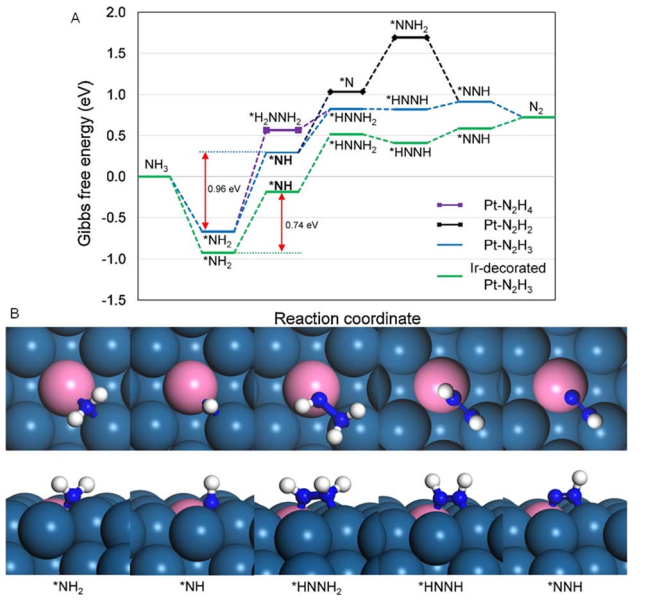

Fig. 9 (A) Gibbs free energy curves for AOR pathways on Pt(100) and Ir-decorated Pt(100) and (B) optimized structures (top and side views) of reaction intermediates using the N_2H_3 route during AOR on Ir-decorated Pt(100). Color code: Ir, pink; Pt, dark blue; H, white; N, blue. Reproduced from ref. 9 with permission from Springer, copyright 2020.

In addition, adding 3D transition metals like PtIrZn and PtIrNi to PtIr alloy increased AOR activity.[43,72] An instance of this can be seen in the PtIrZn electrode, which exhibits a low onset potential of 0.30 V relative to RHE and a high exchange current density of 0.0043 mA cm^{-2}. This indicates that in contrast to the nanostructuration of PtIr, the most probable source is the introduction of Zn. H_2 electrochemistry takes place on Pt-based electrodes between 0 and 0.40 V; therefore, dissociative adsorption of NH_3 ought to compete with H_2 adsorption. The inhibition of competitive H_2 adsorption would be advantageous. This may be accomplished by introducing Zn with a high H_2 overpotential into PtIr.

For PtIrNi, the catalyst showed significantly enhanced AOR activity with a reduced onset potential of approximately 0.40 V, compared to the binary PtIr and bare Pt catalysts. This improvement can be explained by the d-band model. The electronic structure analysis revealed that Ir atoms on the surface have a higher d-band center relative to Pt atoms (−1.97 *vs.* −2.25 eV), resulting in fewer occupied antibonding states and stronger adsorption energies for *NH[72] (Fig. 10A). Adding Ni to the surface further shifts the d-orbital density of states up in energy (−1.97 to −1.87 eV), strengthening the adsorption of *NH intermediates and enhancing AOR activity. This group orbital model theoretically supports the promotional role of Ni in PtIr alloys for improved AOR performance. The Gibbs free energy pathways also supported that with the addition of a Ni atom to the $Pt_3Ir(100)$ surface, the dehydrogenation of $*NH_2$ to *NH becomes exergonic at 0.3 V *vs.* RHE which lowering the thermodynamic barrier in the dehydrogenation process[72] (Fig. 10B).

In addition to promoting alloy formation, Pt-supported metal oxide at the nanoscale can also accelerate the AOR reaction. Ntais *et al.* accomplished the synthesis of platinum nanoparticles that were backed by NiO, MnO_2, and carbon black.[44] As compared to Hg/HgO, Pt/NiO exhibited the greatest current density (0.24 mA cm^{-2}) and the least onset potential for AOR (−0.48 V). Similarly, Pt supported on TiO_2 nanoparticles and embellished with sulfur-doped onion-like carbon nanoparticles (S-OLCNs) exhibited superior resistance to charge transfer and enhanced long-term stability.[45] Pt/TiO_2/S-OLCN demonstrated a current density of 0.28 mA cm^{-2}, which is greater than that of commercial Pt/C. The enhanced catalytic performance of the Pt/TiO_2/S-OLCN electrocatalyst can be attributed to the cohesive metal–support interface formed by the S-OLCN-TiO_2 composite support material and Pt nanoparticles. Additionally, this may be the result of the "spillover" phenomenon, in which intermediates adsorbed on Pt sites migrate to adjacent Ti–OH species to aid in the acceleration of oxidation. TiO helps keep the Pt catalyst from becoming inactivated by N_2 intermediates (Pt–N_{ads}), which are harmful to the Pt that is created during the AOR. In addition, the Pt/TiO_2/S-OLCN catalyst will be more able to catalyse the creation of AOR because the Pt NPs and the S groups in the onion structure

Published on 07 Mhawuri 2024. Downloaded on 2026-05-14 21:13:42.

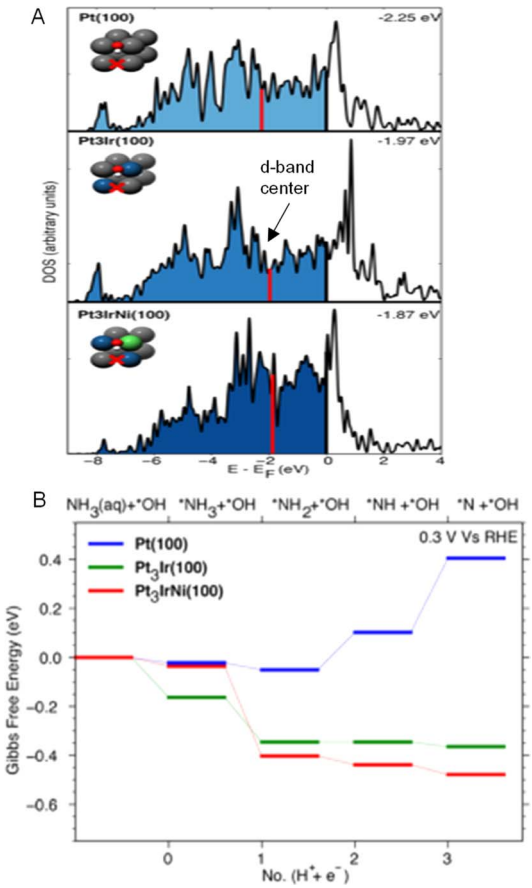

Fig. 10 (A) Group d-orbital density of states projected onto the bridge site of model systems and (B) free-energy pathway *via* constant-potential DFT calculations for initial ammonia dehydrogenation steps at 0.3 V *vs.* RHE on Pt(100), $Pt_3Ir(100)$, $Pt_3IrNi(100)$. Reproduced from ref. 72 with permission from ACS Publications, copyright 2020.

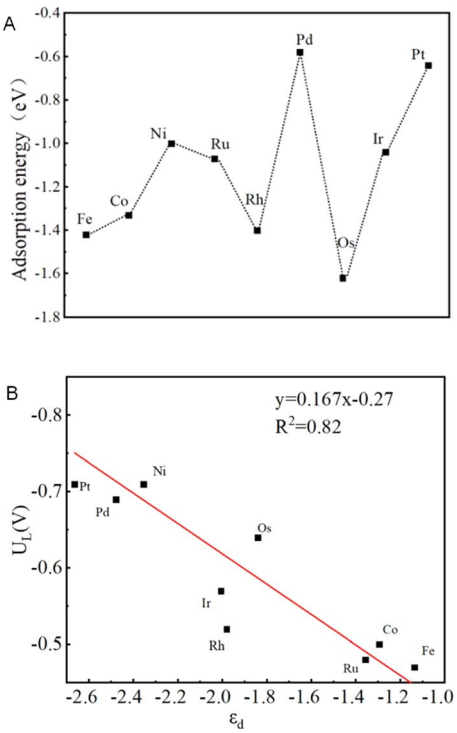

Fig. 11 (A) Adsorption energy of transition metal atoms anchored at a g-CN monolayer (TM_2@g-CN) and (B) the scaling relationship between d band center (ε_d) and the limiting potential (U_L). Reproduced from ref. 46 with permission from Elsevier, copyright 2023.

have robust electron transfer connectivity, which will change the surface's electrical state. Lastly, Barbosa *et al.* reported that $PtSnO_2$ nanoparticles with a preferential (100) orientation significantly decreased the onset potential for the AOR by approximately 70 mV.[14] The high catalytic activity of these materials is attributed to the Pt (100) orientation, which exhibits a higher tolerance for poisoning intermediates like adsorbed nitrogen species (N_{ads}). Additionally, the presence of SnO_2 helps prevent the deactivation of the Pt surface caused by intermediates formed during the AOR.

Recently, Zhong *et al.* conducted a study on a series of transition metal atoms anchored at a g-CN monolayer (TM_2@g-CN), including Fe, Co, Ni, Ru, Rh, Pd, Os, Ir, and Pt, to identify high-performance AOR electrocatalysts.[46] Compared with bulk Pt, the interaction between metal and support on the TM_2@g-CN catalyst leads to a positive charge on the metal atoms, making their corresponding d orbitals easier to polarize and more effective at adsorbing NH_3 (ref. 46) (Fig. 11A). This interaction also accelerates the coupling of dinitrogen, reducing the onset potential of NH_3 oxidation to 0.48–0.52 eV, compared to the experimentally measured onset potential of 0.62 eV for the Pt (100) surface, without producing surface-poisonous nitrogen. Among all TM_2@g-CN electrocatalysts, Fe, Co, Ru, Rh, and Ir anchored in the g-CN monolayer shows the most promise as AOR catalysts due to their low limiting potentials of −0.47, −0.5, −0.48, −0.52, and −0.48 V, respectively. Furthermore, the catalytic performance of these TM_2@g-CN candidates strongly correlate with the d band center (ε_d) of the TM atoms, which is beneficial for designing promising AOR catalysts. When the ε_d shifts closer to the Fermi energy level, the limiting potential (U_L) value becomes less negative, indicating increased activity[46] (Fig. 11B). Therefore, the ε_d can directly predict AOR activity, and a downshift in the metal ε_d helps maintain long-lasting electrocatalytic activity.

Based on the activation energy barrier, the dimerization of NH_2 in Ir_2@g-CN is more favorable than in other metals, with an activation energy of 0.93 eV. The activation energies for the other four TM_2@g-CN catalysts are 2.17, 1.76, 3.3, and 1.59 eV, all higher than the activation energy for the Pt (111) surface, which is 1.07 eV. Referring to the adsorption and activation energy, the mechanism proposed by G–M is kinetically preferred. This mechanism involves N–N bond formation *via* hydrogenated NH_x species rather than N adatoms because the strong adsorption energy of NH_2 on the TM_2@g-CN monolayer requires a large potential for NH_2 deprotonation into NH. Therefore, the N + N mechanism is not considered in this study.

In summary, recent research focuses on optimizing catalyst materials, morphologies, and surface orientations to enhance AOR performance, with a particular emphasis on single-atom catalysts and alloying strategies.

 This journal is © The Royal Society of Chemistry 2024

Published on 07 Mhawuri 2024. Downloaded on 2026-05-14 21:13:42.

Transition metal-based electrocatalysts

Active catalysts in AOR have been regarded as Pt and Pt-based noble metals due to their high N_2 selectivity and low overpotential; nevertheless, their substantial expenses and vulnerability to deactivation have demonstrated themselves to be formidable obstacles. As an alternative to platinum-based electrocatalysts, non-noble metal-based electrocatalysts have been suggested recently. Non-noble metal catalysts, particularly transition metals (*e.g.*, Ni-based compounds, CuO, Ni–Co bimetallic and Ni–Cu), are of interest in AOR for electrolytic H_2 production and effluent cleanup.[73] After conducting a large number of theoretical calculations and practical investigations, it was shown that Ni possesses the highest HER exchange current density and the lowest free energy of H_2 adsorption (*GH) among a wide variety of nonprecious metals. Based on these findings, it appears that Ni could be a potential candidate for significantly increasing the intrinsic activity of HER. On the other hand, Yao *et al.* found that pure nickel had a low amount of AOR activity. This was because pure nickel had a high electrode consumption at the voltage that was required for NH_3 oxidation.[74] It is not possible for NiO to effectively oxidize NH_3 because the negative charge on the cation vacancies causes the generation of reverse electrons, which speeds up the deactivation of the anion.

In a recent study, Almomani *et al.* established that the addition of TiO_2 to a Ni-based electrode substantially improves its efficacy for AOR.[10] The redox potential of Ni(II)/Ni(III) increased from +0.65 to 1.24 V as a result of the pretreatment technique for NiO nanocatalyst. This is in contrast to the redox potential of HgO/Hg, which remained unchanged. The NH_3 oxidation potential is the component that is responsible for this increase. As an additional point of interest, it was observed that a potential of 1.24 V is sufficient to fully facilitate the transition of $Ni(OH)_2$ into NiOOH, which is a situation that encourages the oxidation of NH_3. In the interim, NiO–TiO_2-treated nanopowders demonstrated a notable enhancement in their ability to achieve AOR. As the redox potential for the Ni(II)/Ni(III) reaction increased from +0.72 to 1.35 V, a strongly oxidising environment was formed. This resulted in a rise in the built-on $Ni(OH)_2$ layer, which in turn led to the oxidation of a bigger quantity of NH_3. In fact, metallic Ni and NiOOH are not catalytically active unless they are electrochemically converted to NiOOH at approximately 1.3 V *vs.* RHE. The dehydrogenation of NH_3 begins with an electron-coupled proton transfer to NiOOH, resulting in a would-be reversible reduction of NiOOH to $Ni(OH)_2$.[75] Huang *et al.* reported that Cu_2O wire-in-$Ni(OH)_2$ plate passivated by a thin CuO surface ($Ni(OH)_2$–Cu_2O@CuO) achieves a stable current density as high as ~80 mA cm^{-2} for more than 30 h, demonstrating a much superior AOR performance than the previous works.[51] This novel wire-in-plate nanostructure, featuring intimate contact among $Ni(OH)_2$, Cu_2O, and CuO, develops dual interfaces of $Ni(OH)_2$–Cu_2O and Cu_2O@CuO. These interfaces effectively protect Cu_2O from oxidation and inhibit the dissociation of copper species into the electrolyte. In addition, after adding 1 M NH_3 into the electrolyte, a large current density of ~60 mA cm^{-2} was detected with an onset potential of 0.47 V *vs.* Hg/HgO for 10 mA cm^{-2}.

Similarly, Xu *et al.* found that Cu effectively improve activity of $Ni(OH)_2$ for NH_3 electrooxidation which mixed NiCu layered hydroxides achieve a current density of 35 mA cm^{-2} at 0.55 V *vs.* Ag/AgCl and 0.28 V of onset potential at higher NaOH concentration, which is much higher than that of bare $Ni(OH)_2$ catalyst (5 mA cm^{-2}).[52] This is attributed to the abundant active sites and the synergistic effect between Ni and Cu, likely due to the formation of $Ni_{1-x}Cu_xOOH$ on the surface of the catalysts through the electrochemical activation of the mixture of $Cu(OH)_2$ and $Ni(OH)_2$. Xu *et al.* also claimed that NiOOH is the actual active substance.[76] NiOOH is formed from β-$Ni(OH)_2$ *via* an electrochemical reaction in an alkaline solution to catalyze NH_3 oxidation and then is reduced back to β-$Ni(OH)_2$ (eqn (15) and (16)). This study showed that without Ni element, the Cu catalyst was found to have negligible activity.

$$\beta\text{-Ni(OH)}_2 + OH^- \rightarrow NiOOH + H_2O + e^- \quad (15)$$

$$NiOOH + NH_3 \rightarrow \beta\text{-Ni(OH)}_2 + \text{products} \quad (16)$$

In details, Tsai *et al.* reported that Ni foam (NF) exhibited a redox couple of α-$Ni(OH)_2$(s) ↔ γ-NiOOH(s) at 0.65 V and 0.38 V on the positive and negative scans.[53] However, an irreversible anodic peak at approximately 0.95 V (*vs.* Hg/HgO) was observed when the addition of Cu_2O with different three morphologies of flower, particle, and sheet Cu_2O. This result indicated that the transformation of β-$Ni(OH)_2$(s) to β-NiOOH(s) *via* the oxidation process with the addition of Cu_2O. At anodic peaks around 0.95 V, the electrodes demonstrated varying peak current densities, highlighting their catalytic activity. Flower Cu_2O/NF had the highest peak current density at 4.6 mA cm^{-2}, followed by particle Cu_2O/NF at 3.1 mA cm^{-2}, sheet Cu_2O/NF at 2.2 mA cm^{-2}, and NF at 1.2 mA cm^{-2}. This order reveals that the presence of Cu_2O in combination with NF significantly enhances catalytic activity. In terms of onset potential, it decreased from 0.75 V (for the NF electrode) to 0.55 V for all Cu_2O/NF electrodes. This indicates an increase in the NF electrode's activity towards AOR with the introduction of Cu_2O electrocatalysts.

Co and its composites, which are equally as extensively utilized as Ni, were also the subject of research due to their exceptional H_2 production activity, high electrical conductivity, and durability. After that, the introduction of Co into Ni–C resulted in an improvement in AOR through the reduction of oxidation peaks within the potential range of 0.23–0.56 V, the augmentation of reversible metal-hydroxide production, and the generation of power (P_{gen}) to maintain the reaction.[48] Greeley *et al.* concluded that, in addition to noble metals such as Pt and Ir, transition metals Ni and Co demonstrated high activities for HER.[77]

Metal oxides often suffer from insufficient activity and poor electrical conductivity. However, adding electronegative nonmetals like phosphorus (P) and sulfur (S) can modify the electronic structure of transition metals and accelerate the surface reconstruction of the catalyst. The high electronegativity of S

Published on 07 Mhawuri 2024. Downloaded on 2026-05-14 21:13:42.

attracts electrons from the outer layer of the transition metal. This attraction lowers the energy barrier for reaction intermediates, thereby enhancing the catalytic properties. This approach also significantly enhances the electrical conductivity of the catalysts. For example, a heterostructured electrocatalyst, Ni_3S_4@$NiCo_2O_4$/NF, was synthesized using the hydrothermal method for the AOR reaction.[54] Electrochemical tests indicated that the heterostructure of Ni_3S_4 and $NiCo_2O_4$ enhanced both the electrocatalytic activity and electrical conductivity compared to single-component catalysts, which demonstrated the highest current response and the lowest onset potential of 0.63 V *vs.* Hg/HgO at the current density of 50 mA cm^{-2}. *In situ* Raman spectroscopy revealed that during the AOR process, the surface of the heterostructured catalyst underwent significant reconstruction, forming γ-NiOOH with a more loose and disordered structure. Additionally, the $NiCo_2O_4$ phase facilitated reconstruction at lower potentials. DFT calculations demonstrated that electron transfer within the heterostructured catalysts accelerated the reconstruction process and reduced the energy barriers for Ni_3S_4 and $NiCo_2O_4$ in the $*NHNH_2$ generation step. This promoted NH_3 adsorption and N_2 desorption, resulting in excellent AOR performance and following the G–M mechanism. The production of N_2 in the AOR process represents a rapid energy release mechanism that effectively mitigates critical catalyst poisoning issues.

Recently, engineering confined transition metal nitride nanostructures offers an effective approach to directly control the NH_3 adsorption/desorption process. This is facilitated by their tunable metal composition, excellent conductivity, high corrosion resistance, and large surface area. For example, after conducting electrochemical measurements, it was determined that the 1D nanoneedle Ni–Co_2N electrode exhibited favourable surface area and active sites. This was demonstrated by its near-zero H_2 evolution onset potential, 74 mV overpotential at 10 mA cm^{-2}, 138 mV at 100 mA cm^{-2}, and 67 mV dec^{-1} Tafel slope.[21] Furthermore, it exhibited exceptional long-term stability, as evidenced by a marginal decrease in the rate of H_2 production following a decade of chronoamperometry measurements. In addition, at 100 mA cm^{-2}, the potential of NH_3 electrolysis in a two-electrode system was 0.71 V, which was lower than that of water splitting. This indicates that the H_2 produced from NH_3 electrolysis may represent a viable alternative to water splitting. Interestingly, the incorporation of transition metal nitrides results in a downshift of the metal d-band center.[78] This effectively increases the antibonding electron density in the metal-adsorbate bond, potentially enabling electrocatalysts to achieve targeted moderate metal-adsorbate interactions through d-band contraction. Theoretical simulations indicate that the downshift of the metal d-band on nickel-cobalt nitride ($NiCo_2N$) nanosheets helps maintain long-lasting AOR activity.[15] This is due to the moderate metal–NH_3 bond strength resulting from the d-band center downshift, optimizing key steps in AOR such as NH_3 adsorption and $*N_2$ species desorption. Nitriding metals downshift metal d-bands and create empty e_g and t_{2g} states near the Fermi level. These empty states increase the oxidation states of the metal center and act as electron acceptors, reducing the barrier to generate NH_x^+ cation radicals by facilitating fast electron transfer from the adsorbed NH_x to the high oxidation state metal site. $NiCo_2N$ nanosheets demonstrate lower charge transfer resistance (4.5 Ω) during AOR and a lower onset overpotential of 0.55 V.

Aside from that, the dendrite-like NiCuBO/NF demonstrates exceptional stability and electrocatalytic activity for AOR. Attainment of 25 mA cm^{-2} current density and a Tafel slope of 63 mV dec^{-1} for AOR requires a mere 1.301 V.[49] In a similar vein, boron nanoclusters deposited onto NiFe layered double hydroxide nanosheets (B-NiFe-LDH/NF) demonstrated notable efficacy, as evidenced by a current density of 100 mA cm^{-2} and a voltage of 1.781 V, which is 202 mV lower than the voltage necessary for complete water splitting. Furthermore, after 24 hours of electrolysis, 78.6% of the NH_3 was removed[50] (Fig. 12A and B). Furthermore, the utilization of density functional theory (DFT) simulation revealed that the formation of boron nanoclusters resulted in a reduction of the energy barrier, thereby promoting the NH_3 adsorption–desorption process and the Volmer phase.

Fig. 13A illustrates that the effective AOR activity of TiO/Ti foil is demonstrated in an alkaline NH_3 solution at a current density of 0.06 mA cm^{-2} and a voltage greater than 0.4 V.[32] The surface Vo in TiO is shown to significantly facilitate AOR activity through the reduction of the energy barrier in the rate-determining $-HNNH_2$ formation phase and the promotion of N_2 desorption, as demonstrated by density functional theory (DFT) calculations[32] (Fig. 13B). Defective TiO_2 is a stable and cost-effective catalyst for

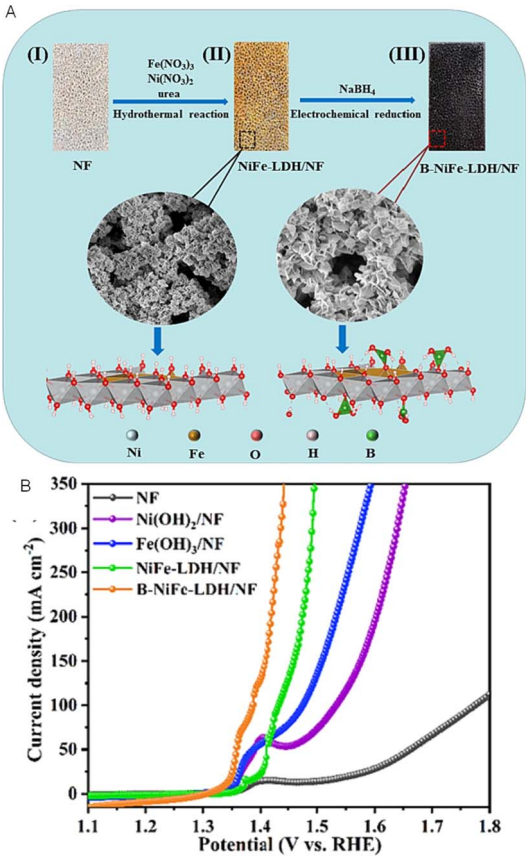

Fig. 12 (A) Schematic diagram and (B) LSV curve of B-NiFe-LDH/NF electrode. Reproduced from ref. 50 with permission from Elsevier, copyright 2023.

This journal is © The Royal Society of Chemistry 2024

Published on 07 Mhawuri 2024. Downloaded on 2026-05-14 21:13:42.

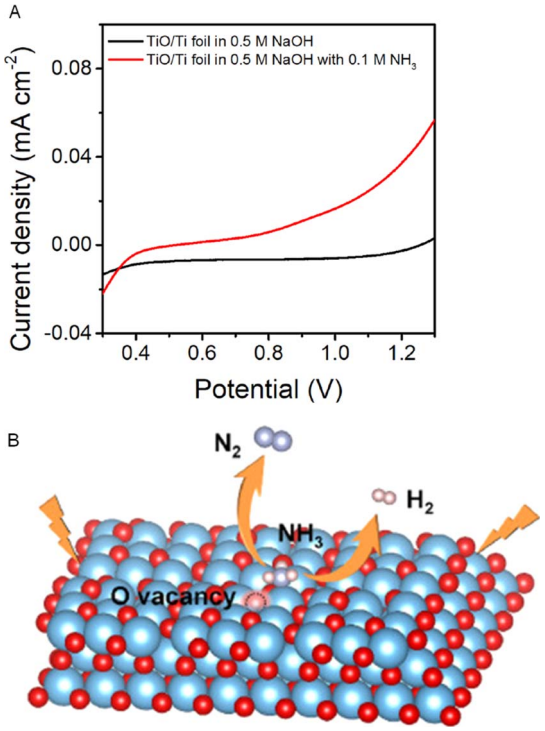

Fig. 13 (A) LSV curves of TiO/Ti foil in 0.5 M NaOH and 0.5 M NaOH with 0.1 M NH_3 solution at a scan rate of 10 mV s^{-1} and (B) schematic diagram of AOR reaction in the presence of an oxygen vacancy on TiO surface. Reproduced from ref. 32 with permission from Elsevier, copyright 2021.

AOR, which is a potential electrode for efficient H_2 production *via* NH_3 electrolysis and direct NH_3 fuel cells, as demonstrated by these results. Similarly, the Vo interfacial site is the main adsorption site for NH_3.[79] Aside from that, Khan *et al.* reported that the half-filled d-orbitals of Pd and Ru promoted ZnO/Al_2O_3 ternary materials as effective and robust electrocatalysts towards AOR.[47] The current density was 0.307 mA cm^{-2} for $PdO/ZnO/Al_2O_3$, which was less than that of $MnO_2/ZnO/Al_2O_3$.

Perovskite oxides, represented by the formula ABO_3, are intriguing electrocatalysts due to their significant chemical and structural flexibility. In an ideal cubic system, the larger A-site is typically occupied by an alkaline-earth metal with 12-fold oxygen coordination, while the smaller B-site is occupied by a transition metal with 6-fold BO_6 oxygen coordination. Zhang *et al.* investigated the use of Ni/Cu in the B-site of a stoichiometric $LaNi_{0.5}Cu_{0.5}O_{3-\delta}$ perovskite as an AOR catalyst.[55] Their findings revealed that annealing the material in an argon atmosphere introduced Vo, which significantly enhanced its catalytic activity (onset potential of 0.55 V *vs.* Ag/AgCl at 10 mA cm^{-2}). Similarly, Jeerh *et al.* investigated the optimal amount of Fe doping in $La_{1-y}Ni_{0.6}Cu_{0.4-x}Fe_xO_{3-\delta}$ and discovered that $La_{0.9}Ni_{0.6}Cu_{0.35}Fe_{0.05}O_{3-\delta}$ exhibited superior activity for the AOR.[56] This was evidenced by a lower onset potential of 0.55 V *vs.* Ag/AgCl at 50 mA cm^{-2}, attributed to the presence of Vo introduced by an A-site deficiency, which led to greater exposure of active Ni^{2+} on the surface. However, compared to the Zhang and co-workers' study, $La_{0.5}Sr_{1.5}Ni_{0.9}Cu_{0.1}O_{4-\delta}$ can act as a robust AOR anode and achieve 13.4 mA cm^{-2} at a lower onset potential of 0.53 V *versus* Ag/AgCl.[57] The selective substitution of La with Sr enhances electronic conductivity and increases Vo concentration. Additionally, doping Cu into the B-site of the perovskite fosters a synergistic interaction between nickel and copper, leading to excellent AOR activity.

Fig. 14 shows the comparison of onset potential for various transition metal electrocatalysts for AOR. Among all catalysts, $RuO_2–ZnO/Al_2O_3$ showed the lowest onset potential, followed by the $Ni_{1-x}Cu_xOOH$. The half-filled d-orbitals of Ru promoted ZnO/Al_2O_3 ternary materials as effective and robust electrocatalysts towards AOR, meanwhile the abundant active sites and the synergistic effect between Ni and Cu, likely due to the formation of $Ni_{1-x}Cu_xOOH$ on the surface of the catalysts through the electrochemical activation of the mixture of $Cu(OH)_2$ and $Ni(OH)_2$. The perovskite oxide also shows a lower onset potential, which is likely due to the presence of Vo, which led to greater exposure of active Ni^{2+} on the surface. Most Ni-based Cu and Co show comparable onset potential for AOR reaction and the larger onset potential is B-NiFe-LDH/NF.

As a conclusion, both single-atom electrocatalysts and transition metal-based electrocatalysts have shown promising performance in NH_3 electrooxidation. However, single-atom electrocatalysts offer several advantages over traditional transition metal-based catalysts, including higher catalytic activity, selectivity, and stability. The unique electronic and geometric structures of single-atom catalysts provide highly active and stable catalytic sites, leading to enhanced NH_3 conversion efficiency and H_2 production selectivity. Additionally, single-atom electrocatalysts can minimize the use of expensive transition metals, reducing production costs and improving the scalability of NH_3 electrooxidation technology.

Techno-economic analysis for NH_3 electrolysis

It is a promising alternative to use NH_3 for the long-distance storage and transportation of H_2 that is produced from renewable sources. An evaluation of the technological and economic

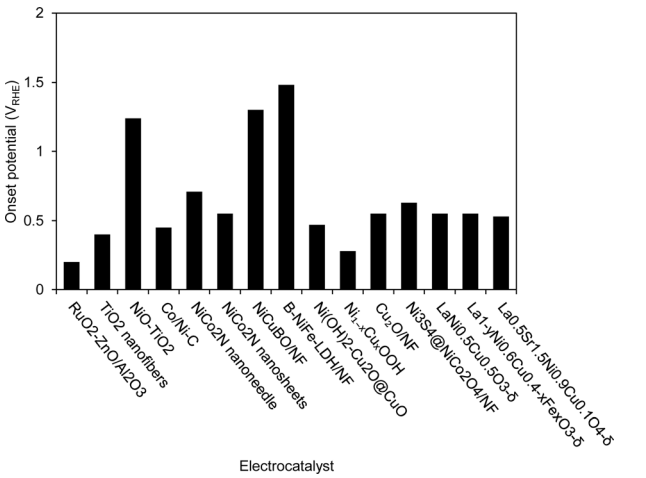

Fig. 14 Comparison of onset potential of various transition metal electrocatalysts under different current densities for AOR.

Published on 07 Mhawuri 2024. Downloaded on 2026-05-14 21:13:42.

aspects was carried out to ascertain the levelized cost of H_2 (LCOH) that is produced from renewable NH_3 feedstocks as tabulated in Table 2. Lee *et al.* conducted a study in which they evaluated the costs that are connected with the thermal breakdown of NH_3 to produce H_2 at two distinct rates which are 0.9 $m^3\ h^{-1}$ (0.08 $kg\ h^{-1}$) for a laboratory scale and 30 $m^3\ h^{-1}$ (2.67 $kg\ h^{-1}$) for a small-scale H_2 refueling station.[80] They established a model of the process in their paper and verified its accuracy by comparing it to experimental findings reported by Chung *et al.*[86] The cost of H_2 production was assessed by the authors through the utilization of various economic methodologies, including sensitivity analysis, profitability analysis, and itemized cost estimation. By utilising itemised cost estimating and beginning with a green NH_3 pricing of 548 USD per tNH_3, they were able to calculate that the LCOH on the laboratory scale was 9.97 USD per kgH_2, while the LCOH on the refuelling station scale was 6.27 USD per kgH_2.[80] These figures correspond to reconversion costs of 6.75 USD per kgH_2 and 3.14 USD per kgH_2, respectively, when the cost of NH_3 feedstock is excluded from the LCOH calculation.

Nasharuddin *et al.* conducted a separate study in which they evaluated the technological and economic feasibility of NH_3 dissociation into H_2 for centralised installations (1000 $kgH_2\ d^{-1}$) and replenishment stations (500 $kgH_2\ d^{-1}$).[81] Due to differences in CAPEX and OPEX for both scales, the authors concluded that breaking NH_3 is economically viable for centralised H_2 production for 5.5 USD per kgH_2.[81] On the other hand, the refuelling station is economically viable for 101 USD per kgH_2. The price of NH_3 was 520 USD per tNH_3, which the authors used as the basis for their study. Furthermore, Lin *et al.* devised a purification system to generate H_2 through thermal decomposition at an on-site H_2 refueling station supplied with NH_3 is 26.7 $kg\ h^{-1}$.[82] Numerous purification configurations, including PSA, membrane, PSA-membrane, and others, were contrasted in terms of H_2 production costs by the authors. Beginning with an NH_3 cost of 540 USD per tNH_3, the authors came to the conclusion that the PSA followed by the membrane purification system produces the most cost-effective H_2 production cost of 5.98 USD per kgH_2.[82] This is equivalent to a reconversion cost of 0.91 USD per kgH_2, which is the most affordable method of producing methane.

Furthermore, for large-scale H_2 production, comprehensive modeling was carried out by Makhloufi and colleagues, who determined that the LCOH was 5.2 USD per kg.[83] This was determined by assuming that the H_2 output rate was 7560 kg h^{-1} and that the price of NH_3 was 488 USD per tNH_3.[83] A techno-economic modeling study was undertaken by Lullo *et al.* to examine 32 H_2 transport systems, which comprised five fluids (hythane, gaseous H_2, NH_3, liquid H_2 and LOHC) and three modes of transportation (vehicle pipeline, and rail).[84] Following the simulation of the process, they concluded that the amount of thermal energy consumed was 4.38 GJ NG per tH_2, while the amount of electrical energy consumed was 81 kW h per tH_2. In their research, the cost of converting H_2 into H_2 (reconversion) was calculated to be 2.61 USD per kgH_2.[84] Cesaro *et al.* assessed the expenses associated with generating electricity from NH_3 *via* various methods, including the conversion of NH_3 to H_2 for fuel cell applications.[87] To determine the energy efficiency and costs associated with the various routes of NH_3 thermal breakdown using a large-scale NH_3 refinery, a techno-economic assessment was carried out. After everything was said and done, they concluded that the levelized cost of energy would be anywhere between 167 and 197 USD per MW h at a plant capacity factor of 25%, presuming that NH_3 would cost 380 USD per tNH_3.

Papadias *et al.* conducted an assessment of the expenses associated with utilizing various liquid H_2 carriers, such as toluene, methanol, and NH_3, to transport H_2.[85] At a rate of 50 tpd, the authors found that NH_3 had the highest production cost (2.2 USD per kgH_2) and the lowest breakdown cost to H_2 (0.61 USD per kgH_2).[85] According to the IEA's "The Future of H_2" report, the anticipated cost of converting NH_3 to H_2 in a centralised facility (15 000 tNH_3 per year) would be 1 USD per kgH_2. However, the report does not provide any specific assumptions regarding the reconversion process.[88]

In a recent study conducted by Kanaan *et al.*, the most economical ways to produce H_2 gas from NH_3 were found to be electrolysis while in transit, thermal decomposition using membrane technology at the import terminal, and a fixed bed at the H_2 refuelling station.[89] Given the significance of the capital cost in conducting the techno-economic assessment, it is imperative to determine the appropriate dimensions for each piece of equipment. They discovered that membrane reactor technology is currently the most cost-effective method for converting NH_3 to H_2 (7.72 USD per kgH_2). The technology exhibits benefit in comparison to traditional fixed bed technologies by its reduced operational expenses. Electrolysis of NH_3 on a truck resulted in the lowest LCOH, at 9.59 USD per kgH_2. Membrane technology has a somewhat higher LCOH (9.14 USD per kgH_2) than fixed bed technology (8.69 USD per kgH_2).[19] The variations in the process configurations for the various scales account for this. The cost of H_2 gas produced at the import terminal using fixed bed and membrane technology is competitive in terms of LCOH, especially when compared to the current green H_2 pricing in Europe, which are 4–8 USD per kgH_2, according to the IEA.

Table 2 Techno-economic for H_2 production *via* AOR

Method	Cost of H_2 production (USD per kgH_2)	Ref.
Thermal decomposition	9.97	80
Thermal decomposition	5.5	81
Membrane purification	5.98	82
Fired NH_3 cracker	5.2	83
Thermal decomposition	2.61	84
Thermal decomposition	2.2	85
Membrane technology	7.72	19
Electrolysis	9.59	
Fixed bed technology	8.69	

Summary, future perspectives, and recommendations

Electrocatalysts play a crucial role in the electrooxidation of NH_3 for clean H_2 production. With the increasing demand for

 This journal is © The Royal Society of Chemistry 2024

Published on 07 Mhawuri 2024. Downloaded on 2026-05-14 21:13:42.

renewable energy sources, electrocatalysis has emerged as a promising method for efficient and sustainable H_2 production. NH_3, with its high H_2 content, has gained attention as a potential carrier for H_2. However, the electrooxidation of NH_3 faces challenges such as low conversion efficiency, poor selectivity, and catalyst degradation. The commercialization of AOR relies on the development of robust and efficient electrocatalysts. Because of their high NH_3 affinity and fast AOR kinetics, Pt electrocatalysts have been investigated in depth using a variety of techniques, including alloying, surface morphology modification, and electrocatalytic reaction optimization. In particular, by successfully lowering the energy barrier, a Pt–Ir greatly enhanced the reaction kinetics of AOR.

There has been a lot of talk about using cheaper, non-noble metal catalysts, especially catalysts based on nickel, as a substitute for Pt. When the affinity of NH_3 and intermediates on Ni and Cu was changed, the Ni–Cu bimetal catalysts showed the most promising activity in terms of reaction rate and stability. Nevertheless, the development of potent new catalysts and their continued search for are essential for the practical implementation of AOR. Particularly to develop non-noble metal electrocatalysts for AOR that are economical, several obstacles must be surmounted. Initially, selective AOR in regions with minimal overpotential is critical. Alternatively, AOR competes with competing reactions such as water oxidation, NH_3 oxidation to NO_3^- or NO_2, and so on, while traditional electrocatalysts based on non-noble metals showed AOR performance at high overpotentials. Conversely, it was discovered that the introduction of heteroatoms into alloys can modify the electronic configuration of catalysts, leading to a decrease in the energy barrier for NH_3 adsorption and eventually a reduction in the overpotential.

Improving AOR requires not just creating catalysts, but also a basic understanding of the reaction mechanism. At present, the AOR mechanism is primarily being studied in relation to its applicability to Pt catalysts. Nevertheless, the specific rate-determining steps or reaction mechanisms may vary among distinct electrocatalyst types. The DFT calculations have been extensively utilized in order to delineate the fundamental effect of the catalytic modification and to propose reaction mechanisms. In light of developments in theoretical inquiry, experimental observation of reaction mechanisms through the monitoring of adsorbed intermediates has become crucial. Recent studies have documented endeavors to examine the true mechanisms of action on electrocatalysts through the utilization of *in situ* or *operando* characterizations. In light of the advancements made thus far, the AOR possesses considerable practical development potential through the integration of device engineering, catalytic modification, and fundamental research.

The replacement of water with liquid NH_3 is another feature that could revolutionize AOR technology for fuel cells. NH_3 only becomes corrosive when reacting with water to generate the caustic OH^-, however, this gas has a far larger energy density and is resistant to pipeline corrosion. The challenges associated with water oxidation are eliminated when a nonaqueous electrolyte is combined with liquid NH_3. Furthermore, it is critical to conduct further mechanistic investigations on nonaqueous liquid NH_3, given its considerable potential provided that the challenges impeding its application in AOR can be resolved. Aside from this, the efficient energy generation *via* direct NH_3 fuel cells and the electrochemical synthesis of "green NH_3" presents a highly promising pathway towards carbon neutrality by 2050.

Data availability

The data that support the findings of this study are available from the corresponding author upon reasonable request. Please note that due to confidentiality agreements, certain restrictions apply to the availability of the data.

Conflicts of interest

The authors stated that there are no known conflicts of interest in this article.

Acknowledgements

The authors are gratefully acknowledging to the Universiti Teknologi Malaysia for the Fundamental Research Grant (No. 22H51) and Professional Development Research University Grant (No. 06E92 and PY/2024/00993).

References

1 J. A. Okolie, B. R. Patra, A. Mukherjee, S. Nanda, A. K. Dalai and J. A. Kozinski, *Int. J. Hydrogen Energy*, 2021, **46**, 8885–8905.
2 A. Kovač, M. Paranos and D. Marciuš, *Int. J. Hydrogen Energy*, 2021, **46**, 10016–10035.
3 S. Anwar, F. Khan, Y. Zhang and A. Djire, *Int. J. Hydrogen Energy*, 2021, **46**, 32284–32317.
4 L. Cao, I. K. M. Yu, X. Xiong, D. C. W. Tsang, S. Zhang, J. H. Clark, C. Hu, Y. H. Ng, J. Shang and Y. S. Ok, *Environ. Res.*, 2020, **186**, 109547.
5 G. Franchi, M. Capocelli, M. De Falco, V. Piemonte and D. Barba, *Membranes*, 2020, **10**, 10.
6 S. A. Lee, M. G. Lee and H. W. Jang, *Sci. China Mater.*, 2022, **65**, 3334–3352.
7 J. Łuczak and M. Lieder, *Adv. Colloid Interface Sci.*, 2023, **319**, 102963.
8 Y. Tian, Z. Mao, L. Wang and J. Liang, *Small Struct.*, 2023, **4**, 2200266.
9 K. Siddharth, Y. Hong, X. Qin, H. J. Lee, Y. T. Chan, S. Zhu, G. Chen, S.-I. Choi and M. Shao, *Appl. Catal., B*, 2020, **269**, 118821.
10 F. Almomani, R. Bhosale, M. Khraisheh, A. Kumar and M. Tawalbeh, *Int. J. Hydrogen Energy*, 2020, **45**, 10398–10408.
11 R. Wang, H. Liu, K. Zhang, G. Zhang, H. Lan and J. Qu, *Chem. Eng. J.*, 2021, **404**, 126795.
12 M.-H. Tsai, T.-C. Chen, Y. Juang, L.-C. Hua and C. Huang, *Electrochem. Commun.*, 2020, **121**, 106875.

Published on 07 Mhawuri 2024. Downloaded on 2026-05-14 21:13:42.

13 F. Quan, G. Zhan, B. Zhou, C. Ling, X. Wang, W. Shen, J. Li, F. Jia and L. Zhang, *J. Environ. Sci.*, 2023, **125**, 544–552.
14 J. R. Barbosa, M. N. Leon, C. M. Fernandes, R. M. Antoniassi, O. C. Alves, E. A. Ponzio and J. C. M. Silva, *Appl. Catal., B*, 2020, **264**, 118458.
15 S. He, Y. Chen, M. Wang, H. Nuomin, P. Novello, X. Li, S. Zhu and J. Liu, *Nano Energy*, 2021, **80**, 105528.
16 Z.-H. Lyu, J. Fu, T. Tang, J. Zhang and J.-S. Hu, *EnergyChem*, 2023, **5**, 100093.
17 J. H. Jang, S. Y. Park, D. H. Youn and Y. J. Jang, *Catalysts*, 2023, **13**, 803.
18 P. Peng, J. Su and H. Breunig, *Energy Convers. Manage.*, 2023, **288**, 117166.
19 R. Kanaan, P. H. Affonso Nóbrega, P. Achard and C. Beauger, *Renewable Sustainable Energy Rev.*, 2023, **188**, 113784.
20 H. Mashhadimoslem, M. Safarzadeh Khosrowshahi, M. Delpisheh, C. Convery, M. Rezakazemi, T. M. Aminabhavi, M. Kamkar and A. Elkamel, *Chem. Eng. J.*, 2023, **474**, 145661.
21 K. Jiang, K. Li, Y.-Q. Liu, S. Lin, Z. Wang, D. Wang and Y. Ye, *Electrochim. Acta*, 2022, **403**, 139700.
22 N. Hassan, A. Jalil, N. Khusnun, A. Ahmad, T. Abdullah, R. Kasmani, N. Norazahar, M. Kamaroddin and D. Vo, *Environ. Chem. Lett.*, 2022, 1–23.
23 M. Sawal, A. Jalil, T. Abdullah, N. Khusnun, N. Hassan, F. Aziz, A. Fauzi, M. Kamaroddin, M. Omar and S. Haron, *Energy Convers. Manage.*, 2022, **274**, 116456.
24 X. Yang, H. Sun, C. Liu, L. Yu and H. Chen, *Chem. Eng. J.*, 2022, **442**, 136167.
25 N. M. Adli, H. Zhang, S. Mukherjee and G. Wu, *J. Electrochem. Soc.*, 2018, **165**, J3130–J3147.
26 Y. Tian, H. Tan, X. Li, J. Jia, Z. Mao, J. Liu and J. Liang, *Chin. J. Catal.*, 2024, **56**, 25–50.
27 H. Kim, S. Hong, H. Kim, Y. Jun, S. Y. Kim and S. H. Ahn, *Appl. Mater. Today*, 2022, **29**, 101640.
28 K. Siddharth, Y. Chan, L. Wang and M. Shao, *Curr. Opin. Electrochem.*, 2018, **9**, 151–157.
29 X. Jiang, D. Ying, X. Liu, M. Liu, S. Zhou, C. Guo, G. Zhao, Y. Wang and J. Jia, *Electrochim. Acta*, 2020, **345**, 136157.
30 J. Huang, Z. Chen, J. Cai, Y. Jin, T. Wang and J. Wang, *Nano Res.*, 2022, **15**, 5987–5994.
31 X. Yang, L. Sun, X. Liu, Z. Yang, H. Sun, W. Liu and H. Chen, *ACS Catal.*, 2024, **14**, 6236–6246.
32 S. Zhang, Y. Zhao, L. Yan, H. Jiang, X. Yang, Y. Wang, H. Song and X. Zhao, *Int. J. Hydrogen Energy*, 2021, **46**, 39208–39215.
33 N. Akagi, K. Hori, H. Sugime, S. Noda and N. Hanada, *J. Catal.*, 2022, **406**, 222–230.
34 D. T. Tran, T. H. Nguyen, H. Jeong, P. K. L. Tran, D. Malhotra, K. U. Jeong, N. H. Kim and J. H. Lee, *Nano Energy*, 2022, **94**, 106929.
35 C. Jo, S. Surendran, M.-C. Kim, T.-Y. An, Y. Lim, H. Choi, G. Janani, S. Cyril Jesudass, D. Jun Moon, J. Kim, J. Young Kim, C. Hyuck Choi, M. Kim, J. Kyu Kim and U. Sim, *Chem. Eng. J.*, 2023, **463**, 142314.
36 J. H. Jang, S. Y. Park, D. H. Youn and Y. J. Jang, *Catalysts*, 2023, **13**, 803.
37 J. Liu, W. Hu, C. Zhong and Y. F. Cheng, *J. Power Sources*, 2013, **223**, 165–174.
38 N. N. Fomena, S. Garbarino, E. Bertin, A. Korinek, G. Botton, L. Roué and D. Guay, *J. Catal.*, 2017, **354**, 270–277.
39 V. A. Ribeiro, I. C. de Freitas, A. O. Neto, E. V. Spinacé and J. C. M. Silva, *Mater. Chem. Phys.*, 2017, **200**, 354–360.
40 X. Lin, X. Zhang, Z. Wang, X. Zhu, J. Zhu, P. Chen, T. Lyu, C. Li, Z. Q. Tian and P. K. Shen, *J. Colloid Interface Sci.*, 2021, **601**, 1–11.
41 H. Yang, X. Huang, Z. Liu, X. Lin, Q. Chen, J. Li, C. Zhang, Z. P. Kan, Z. Q. Tian and P. K. Shen, *J. Colloid Interface Sci.*, 2023, **652**, 1764–1774.
42 J. C. M. Silva, S. Ntais, É. Teixeira-Neto, E. V. Spinacé, X. Cui, A. O. Neto and E. A. Baranova, *Int. J. Hydrogen Energy*, 2017, **42**, 193–201.
43 J. Jiang, *Electrochem. Commun.*, 2017, **75**, 52–55.
44 S. Ntais, A. Serov, N. I. Andersen, A. J. Roy, E. Cossar, A. Allagui, Z. Lu, X. Cui, E. A. Baranova and P. Atanassov, *Electrochim. Acta*, 2016, **222**, 1455–1463.
45 L. L. Sikeyi, L. R. Bila, T. D. Ntuli, C. T. Selepe, N. W. Maxakato, N. J. Coville and M. S. Maubane-Nkadimeng, *Diamond Relat. Mater.*, 2023, **132**, 109612.
46 J.-J. Zhong, S.-P. Huang, J.-F. Gu, Y. Li, K.-N. Ding, Y.-F. Zhang, W. Lin and W.-K. Chen, *Appl. Surf. Sci.*, 2023, **609**, 155280.
47 S. Khan, S. S. Shah, A. B. Yurtcan, A. A. A. Bahajjaj, A. Zafar and N. K. Janjua, *Fuel*, 2023, **347**, 128446.
48 F. Almomani and M. A. H. S. Saad, *Int. J. Hydrogen Energy*, 2021, **46**, 4678–4690.
49 A. A. Kashale, C.-T. Wu, H.-F. Hsu and I.-W. P. Chen, *Chem. Eng. J.*, 2023, **474**, 145907.
50 J. Wang, S. Qing, X. Tong, K. Zhang, G. Luo, J. Ding and L. Xu, *Appl. Surf. Sci.*, 2023, **640**, 158330.
51 J. Huang, J. Cai and J. Wang, *ACS Appl. Energy Mater.*, 2020, **3**, 4108–4113.
52 W. Xu, R. Lan, D. Du, J. Humphreys, M. Walker, Z. Wu, H. Wang and S. Tao, *Appl. Catal., B*, 2017, **218**, 470–479.
53 M.-H. Tsai, Y. Juang, C.-C. Hu, L.-C. Hua and C. Huang, *J. Environ. Chem. Eng.*, 2024, **12**, 112339.
54 L. Wang, K. Jiang, Z. Wang, T. Li, D. Wang and Y.-Q. Liu, *Chem. Eng. J.*, 2024, **492**, 152268.
55 M. Zhang, H. Li, X. Duan, P. Zou, G. Jeerh, B. Sun, S. Chen, J. Humphreys, M. Walker and K. Xie, *Adv. Sci.*, 2021, **8**, 2101299.
56 G. Jeerh, P. Zou, M. Zhang, S. Chen, J. Humphreys and S. Tao, *Sep. Purif. Technol.*, 2022, **297**, 121451.
57 M. Zhang, P. Zou, G. Jeerh, B. Sun, M. Walker and S. Tao, *Adv. Funct. Mater.*, 2022, **32**, 2204881.
58 H. Li, W. Wang, S. Xue, J. He, C. Liu, G. Gao, S. Di, S. Wang, J. Wang and Z. Yu, *J. Am. Chem. Soc.*, 2024, **146**, 9124–9133.
59 H. Li, S. Di, P. Niu, S. Wang, J. Wang and L. Li, *Energy Environ. Sci.*, 2022, **15**, 1601–1610.
60 C. Liu, F. Yang, A. Schechter and L. Feng, *Adv. Sens. Energy Mater.*, 2023, 100055.
61 F. J. Vidal-Iglesias, J. Solla-Gullón, V. Montiel, J. Feliu and A. Aldaz, *J. Power Sources*, 2007, **171**, 448–456.

 This journal is © The Royal Society of Chemistry 2024

Published on 07 Mhawuri 2024. Downloaded on 2026-05-14 21:13:42.

62 H. S. Pillai and H. Xin, *Ind. Eng. Chem. Res.*, 2019, **58**, 10819–10828.
63 C. Xiao, B.-A. Lu, P. Xue, N. Tian, Z.-Y. Zhou, X. Lin, W.-F. Lin and S.-G. Sun, *Joule*, 2020, **4**, 2562–2598.
64 F. J. Vidal-Iglesias, J. Solla-Gullón, P. Rodrıguez, E. Herrero, V. Montiel, J. Feliu and A. Aldaz, *Electrochem. Commun.*, 2004, **6**, 1080–1084.
65 S. Johnston, B. H. Suryanto and D. R. MacFarlane, *Electrochim. Acta*, 2019, **297**, 778–783.
66 J. Zhou, J. S. Chung and S. G. Kang, *Int. J. Hydrogen Energy*, 2024, **58**, 745–752.
67 M. H. Assumpção, S. G. da Silva, R. F. de Souza, G. S. Buzzo, E. V. Spinacé, A. O. Neto and J. C. M. Silva, *Int. J. Hydrogen Energy*, 2014, **39**, 5148–5152.
68 M. H. Assumpção, R. M. Piasentin, P. Hammer, R. F. De Souza, G. S. Buzzo, M. C. Santos, E. V. Spinacé, A. O. Neto and J. C. M. Silva, *Appl. Catal., B*, 2015, **174**, 136–144.
69 T. L. Lomocso and E. A. Baranova, *Electrochim. Acta*, 2011, **56**, 8551–8558.
70 Q. Xue, Y. Zhao, J. Zhu, Y. Ding, T. Wang, H. Sun, F. Li, P. Chen, P. Jin and S. Yin, *J. Mater. Chem. A*, 2021, **9**, 8444–8451.
71 A. Estejab and G. G. Botte, *Mol. Catal.*, 2018, **445**, 279–292.
72 Y. Li, X. Li, H. S. Pillai, J. Lattimer, N. Mohd Adli, S. Karakalos, M. Chen, L. Guo, H. Xu and J. Yang, *ACS Catal.*, 2020, **10**, 3945–3957.
73 A. Allagui, S. Sarfraz and E. A. Baranova, *Electrochim. Acta*, 2013, **110**, 253–259.
74 K. Yao and Y. Cheng, *Mater. Chem. Phys.*, 2008, **108**, 247–250.
75 J. Łuczak and M. Lieder, *Adv. Colloid Interface Sci.*, 2023, 102963.
76 W. Xu, D. Du, R. Lan, J. Humphreys, D. N. Miller, M. Walker, Z. Wu, J. T. Irvine and S. Tao, *Appl. Catal., B*, 2018, **237**, 1101–1109.
77 J. Greeley, T. F. Jaramillo, J. Bonde, I. Chorkendorff and J. K. Nørskov, *Nat. Mater.*, 2006, **5**, 909–913.
78 D. J. Little, D. O. Edwards, M. R. Smith III and T. W. Hamann, *ACS Appl. Mater. Interfaces*, 2017, **9**, 16228–16235.
79 H. Sun, H. Wang and Z. Qu, *ACS Catal.*, 2023, **13**, 1077–1088.
80 B. Lee, J. Park, H. Lee, M. Byun, C. W. Yoon and H. Lim, *Renewable Sustainable Energy Rev.*, 2019, **113**, 109262.
81 R. Nasharuddin, M. Zhu, Z. Zhang and D. Zhang, *Int. J. Hydrogen Energy*, 2019, **44**, 14445–14455.
82 L. Lin, Y. Tian, W. Su, Y. Luo, C. Chen and L. Jiang, *Sustainable Energy Fuels*, 2020, **4**, 3006–3017.
83 C. Makhloufi and N. Kezibri, *Int. J. Hydrogen Energy*, 2021, **46**, 34777–34787.
84 G. Di Lullo, T. Giwa, A. Okunlola, M. Davis, T. Mehedi, A. Oni and A. Kumar, *Int. J. Hydrogen Energy*, 2022, **47**, 35293–35319.
85 D. D. Papadias, J.-K. Peng and R. K. Ahluwalia, *Int. J. Hydrogen Energy*, 2021, **46**, 24169–24189.
86 D. B. Chung, H. Y. Kim, M. Jeon, D. H. Lee, H. S. Park, S. H. Choi, S. W. Nam, S. C. Jang, J.-H. Park and K.-Y. Lee, *Int. J. Hydrogen Energy*, 2017, **42**, 1639–1647.
87 Z. Cesaro, M. Ives, R. Nayak-Luke, M. Mason and R. Bañares-Alcántara, *Appl. Energy*, 2021, **282**, 116009.
88 IEA, *The Future Hydrogen*, 2019, DOI: **10.1787/1e0514c4-en**.
89 R. Kanaan, P. H. A. Nóbrega, P. Achard and C. Beauger, *Renewable Sustainable Energy Rev.*, 2023, **188**, 113784.